

Catalysis Preparation of Biodiesel from Waste *Schisandra chinensis* Seed Oil with the Ionic Liquid Immobilized in a Magnetic Catalyst: $\text{Fe}_3\text{O}_4@\text{SiO}_2@[\text{C4mim}]\text{HSO}_4$

Jintao Yu, Yinhang Wang, Luqi Sun, Zhou Xu, Yadong Du, Huiliang Sun, Wei Li, Sha Luo, Chunhui Ma,* and Shouxin Liu*



Cite This: *ACS Omega* 2021, 6, 7896–7909



Read Online

ACCESS |



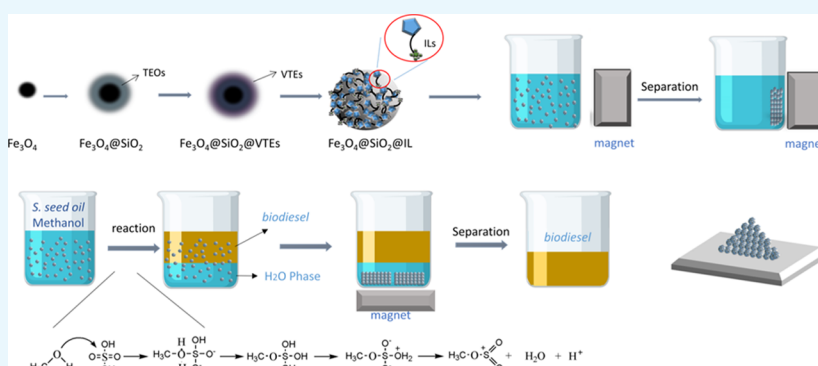
Metrics & More



Article Recommendations



Supporting Information



ABSTRACT: The purpose of this study was to synthesize a magnetic material that could be easily separated by a magnetic field and combined the catalytic function of an acid/base ionic liquid with silicon for biodiesel preparation. A kind of magnetic catalyst-immobilized ionic liquid was synthesized by a three-step method. The synthesis conditions in each step were optimized by single-factor analysis. Under the optimum conditions, 206.83 mg of ionic liquid (>43.63%) was immobilized on SiO_2 (per gram). Heating under reflux was applied to extract *Schisandra chinensis* seed oil with an average yield of 10.9%. According to the biodiesel yields, $\text{Fe}_3\text{O}_4@\text{SiO}_2@[\text{C4mim}]\text{HSO}_4$ was the most efficient catalyst in the methyl esterification reaction. Under the optimum reaction conditions, seed oil (10.0 g) was mixed with methanol (70 mL) under continuous mechanical stirring for 3 h, and the yield of biodiesel was 0.557 g/g (the catalyst efficiency was about 89.2%). Also, the thermal value was increased from 32.14 kJ/g (seed oil) to 38.28 kJ/g (biodiesel). The catalytic efficiency of $\text{Fe}_3\text{O}_4@\text{SiO}_2@[\text{C4mim}]\text{HSO}_4$ was 87.6% of the first being used after four reuse cycles, and 71.4% of the first being used after six reuse cycles in the methylation reaction. The yields and physical and chemical properties of biodiesel were determined.

1. INTRODUCTION

Due to the deterioration of the environment caused by the massive use of fossil fuels, such as global warming and emission of greenhouse gases, identification of suitable alternative fuels is necessary. The use of more renewables, including solar,^{1–3} hydro,⁴ tidal,⁵ wind,^{6,7} and geothermal,⁸ to meet the energy needs of society can reduce the dependence on imported fossil fuels. However, the fuels consumed by some large machines with high energy requirements, such as airplanes, cannot be replaced by these energy sources, and fuel is still indispensable in the near future.^{9–11}

Therefore, alternatives are constantly being sought. However, compared with petro-diesel, biodiesel does not seem to be feasible as its raw materials are costly. Thus, to minimize the production cost of biodiesel, low-price raw materials (waste cooking oil and rapeseed oil, waste animal oils such as lard and butter) are required to convert it into biodiesel and reduce

processing costs. The main components of rapeseed oil, soybean oil, jatropha oil, and animal oils such as lard and butter are triglycerides, which have high viscosities and flash points and are not suitable for burning.¹² Triglycerides cannot meet the work requirements of power equipment,^{13,14} and they can be made into biodiesel. Biodiesel is a green energy source with a high cetane number (63.1)^{15,16} that is flammable, renewable, has a low sulfur content, a high flash point (98.2 °C), low viscosity (2.26 mm (2) s (–1), 40 °C),¹⁷ and low

Received: January 27, 2021

Accepted: February 25, 2021

Published: March 9, 2021



combustion residual carbon.^{18,19} Biodiesel could effectively reduce the consumption of petrochemical resources. The preparation of biodiesel is accomplished by catalytic esterification.^{20,21} The main catalysts used for preparing biodiesel by esterification are homogeneous catalysts, such as inorganic acids and bases, and heterogeneous catalysts,²² for example, molecular sieve catalysts,²³ solid acids,²⁴ and solid bases.²⁵ Homogeneous catalysts, such as alkalis and acids, cause equipment corrosion and are difficult to separate from the solvents.²⁶ Furthermore, the presence of high FFA in the feedstock is undesirable as it could lead to side reactions with the alkaline catalyst to produce soaps. In addition, the separation and recovery of the catalyst also become significantly more difficult, which increases the separation cost. The small pore sizes of molecular sieve catalysts are not conducive to the diffusion and adsorption of fatty acids and triglycerides, and strong acid resins are inactivated at high reaction temperatures and are expensive.²⁷ With heteropoly acids, formation of a liquid phase occurs easily in the reaction,²⁸ which is not conducive for catalyst recycling. After reaction with a solid base catalyst, it is difficult to separate the catalyst and the product and the fatty acid in the oil cannot be effectively converted.^{29,30}

Ionic liquids have low vapor pressures, wide temperature ranges for liquefaction, wide electrochemical windows, excellent electrical conductivity, and adjustable acidity and structures.^{31–34} Therefore, ionic liquids have received considerable attention for use in research and fields³⁵ such as catalysis, separation science, and electrochemistry.^{36,37} Many research studies have proved that ionic liquids can be used for the synthesis of biodiesel.^{38–40} They have the following advantages of inorganic liquid acids and solid acids: good fluidity, high acid density, uniform acid strength distribution, high stability, reusability, and adjustable acid strength. These advantages are beneficial in catalyst research. Most of the homogeneous catalysts reported in the literature have been conventional ionic liquids. In the process of biodiesel synthesis, ionic liquids were difficult to separate,⁴¹ so it is necessary to find a stable catalyst with high activity that is also easy to separate. Immobilized ionic liquids have the following advantages: the ionic liquid becomes a solid after immobilization^{42,43} and is easily separated from the product at a low cost;⁴⁴ an ionic liquid dispersed on the surface of a solid carrier has a large specific surface area, which reduces the ionic liquid requirements and cost and improves the economic feasibility.^{45,46} Also, the catalytic activity is good, continuous catalytic conversion can be realized, and the production capacity is improved. Recent studies have shown that magnetic separation is effective.^{47–49}

There have been many challenges to environmental protection in recent years with further industrialization and urbanization. Among pollution-causing industries, pollution caused by chemicals is also one of the major environmental issues that has also received increasing attention from countries worldwide. Therefore, it is also important for laboratories to solve the problem of reagent waste and environmental pollution in practical applications.

The purpose of this study was to synthesize a magnetic material that could be separated easily by a magnetic field and combined the catalytic function of an acid–base ionic liquid with silicon. In this way, not only can bio-oil be converted into diesel but also the recovery problem of resource can be solved and the environmental pollution caused by catalyst emissions

can be avoided. In this experiment, an acidic ionic liquid was selected to provide an acidic site to catalyze the synthesis of biodiesel from methanol and seed oil. The catalyst was applied to prepare biodiesel from *Schisandra chinensis* seed oil with a high catalytic efficiency.

2. RESULTS AND DISCUSSION

2.1. Single-Factor Analysis of the Magnetic Immobilized Ionic Liquid Preparation.

2.1.1. Effect of the Mixing Speed. The mixing rotational speed is an extremely important factor that can affect the particle size and the specific surface area of the catalyst surface, and the increase of the specific surface area will indirectly affect the amount of ionic liquid bonding; however, when the rotational speed reaches a certain speed, the bonding quantity has little effect. In this experiment, a stepless speed agitator was used (Table 1). As the rotation

Table 1. Effect of Rotation Speed on Loading Quality

no.	speed (rpm)	Fe ₃ O ₄ (g)	yield of synthesis Fe ₃ O ₄ @SiO ₂ (g)
1	250	1.5008	1.8005
2	350	1.5020	2.2093
3	450	1.5016	2.2101

speed was increased from 250 to 350 rpm, the product yield increased by 22.7%. Above 350 rpm, the increase in the Fe₃O₄@SiO₂ yield was minimal (1.21%). According to these results, a rotation speed of 350 rpm was selected for subsequent experiments.

2.1.2. Effect of the Volume of TEOS. As the volume of TEOS increased, the yield of Fe₃O₄@SiO₂ also increased (Figure 1a). The maximum thickness of the silica gel layer was not reached if the TEOS volume was insufficient. Consequently, the adhesion of the silica gel improved, and the yield of the product increased with an increase in the volume of TEOS. When the volume of TEOS exceeded 5.0 mL, the quantity loaded on the Fe₃O₄@SiO₂ hardly increased because the TEOS was present in excess. When the weight of Fe₃O₄ was 1.50 g, the optimum volume of TEOS was 5.0 mL.

2.1.3. Effect of VTES. The effects of different amounts of VTES (Figure 1b) on the yield of modified magnetic SiO₂ particles were investigated. When the amount of VTES was increased from 5.0 to 10.0 mmol, the yield of Fe₃O₄@SiO₂@VTES particles increased significantly. Further increases in the VTES amount did not result in increases in the yield of Fe₃O₄@SiO₂@VTES particles. Therefore, 10.0 mmol VTES was selected as the optimum amount.

2.1.4. Effect of the Dosages of Ionic Liquid. The ionic liquid used in this experiment was 1-butyl-3-methyl-imidazole ([C4mim]OH), which has a molecular weight of 156.23. When the weight of the ionic liquid was increased from 0.50 to 1.50 g, the quantity loaded on the ionic liquid increased greatly (Figure 1c), but no significant differences were observed in the synthesized magnetic particles when the weight of the ionic liquid was increased from 1.50 to 3.00 g. The limited pore space inside the silica gel restricts the mass of the ionic liquid that can be immobilized. Initially, the ionic liquid cannot occupy the entire binding site, and the amount of the ionic liquid immobilized is less than the mass of VTES. The mass of [C4mim]OH (1.50 g) was a little less than 10 mmol. Therefore, the optimum amount of the ionic liquid for the synthesis of the immobilized ionic liquid catalyst was 10 mmol.

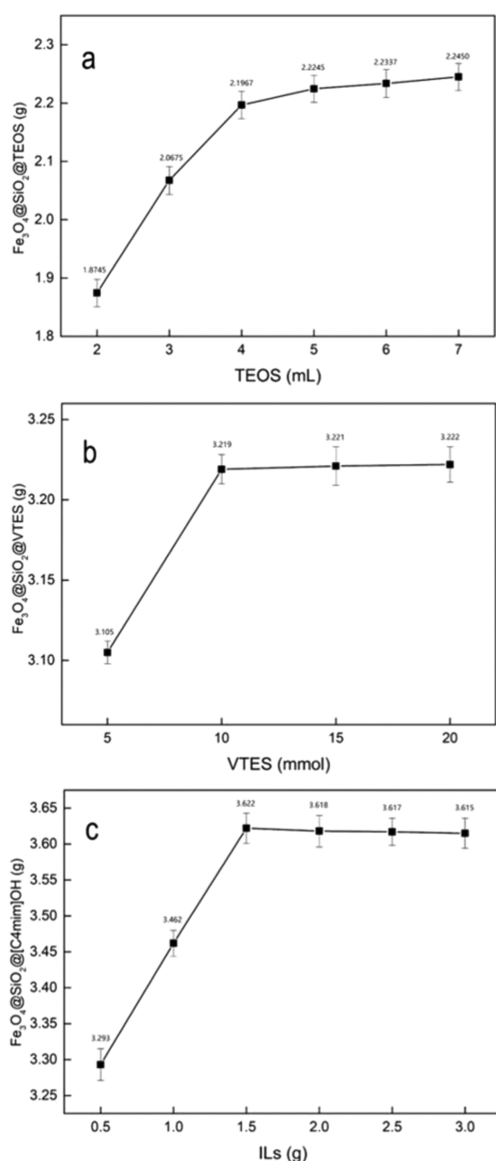


Figure 1. Single-factor analysis of Fe₃O₄@SiO₂@[C4mim]OH preparation. (a) Effect of TEOS volume on the quantity loaded on Fe₃O₄@SiO₂. (b) Effect of the amount of VTES on the quantity loaded on Fe₃O₄@SiO₂@VTES. (c) Effect of IL dose on the quantity loaded on Fe₃O₄@SiO₂@[C4mim]OH.

2.1.5. Ionic Liquid Loading Capacity on the Magnetic Carrier. The average weight of [C4mim]OH loaded on the magnetic particles was calculated to be 206.83 ± 12.13 mg/g (Table 2). During the synthesis of the catalyst, about 1.50 g of the ionic liquid [C4mim]OH was added. At least 43.63% of the ionic liquid monomer was fixed in the VTES-modified magnetic SiO₂ particles (Table 2). These results indicated that

Table 2. Loading Capacity of [C4mim]OH

no.	addition of [C4mim]OH (g)	weight before loading (g)	weight after loading (g)	loading of ILs (mg/g)
1	1.50	3.0003	3.6259	207.63
2	1.50	3.0013	3.5854	194.70
3	1.50	3.0007	3.6552	218.16
average				206.83

if the amount of ionic liquid was higher, the catalytic performance of the catalyst was stronger.

2.1.6. Loading Quantities with Different Types of Ionic Liquids. In this experiment, multiple ionic liquids with different anions and cations were used. Fe₃O₄@SiO₂@VTES particles (3.00 g) were mixed with 10 mmol of an ionic liquid (Table 3). Each experiment was repeated three times to obtain the

Table 3. Loading Capacity of Different Types of Ionic Liquids

no.	ionic liquid	acidity or alkalinity	weight of IL (g)	weight before loading (g)	weight after loading (g)	loading ratio of ILs (%)
1	[C4mim]HSO ₄	acidic	2.36	3.0009	3.5785	24.47
2	[C4mim]CH ₂ -C ₆ H ₄ ⁻ HSO ₃	acidic	3.10	3.0003	3.7161	23.09
3	[C4mim]NO ₃	acidic	2.01	3.0005	3.6940	34.50
4	[C4mim]OH	alkaline	1.56	3.0003	3.6259	40.10
5	[C4mim]Ac	alkaline	1.98	3.0006	3.7258	36.63
6	[C2mim]Br	neutral	1.91	3.0002	3.5802	30.37
7	[C3mim]Br	neutral	2.02	3.0003	3.5210	25.78
8	[C4mim]Br	neutral	2.19	3.0007	3.7108	32.42
9	[C6mim]Br	neutral	2.47	3.0008	3.6455	26.10
10	[C8mim]Br	neutral	2.75	3.0004	3.5648	20.52
11	[C10mim]Br	neutral	3.03	3.0007	3.8453	27.87

average. Both the cation and the anion influence the chemical polarity. However, the effect of anions is more significant.³⁵ Hence, when the anion was the same (Br), the average percentage of [C4mim]Br (short chain in the cation) loaded on the magnetic particles was higher in the aqueous phase (32.42%) than those of other ionic liquids with different cations. When the cation was the same ([C4mim]⁺), the average percentage of [C4mim]OH (stronger hydrophilicity) loaded on the magnetic particles was higher (40.10%) than those of other ionic liquids with different anions.

2.2. Characterization of the Magnetic Immobilized Ionic Liquid Catalyst.

2.2.1. SEM with EDX. Figure 2 shows the SEM results and the energy of elements for particles from the three synthetic steps for the production of the magnetic immobilized ionic liquid catalyst. The Fe₃O₄@SiO₂ image (Figure 2a) showed that the particles were smooth spheres with nonuniform sizes. Also, the EDX analysis of Fe₃O₄@SiO₂ (Figure 2d) showed the Fe, Si, and O elements. The Fe₃O₄@SiO₂@VTES particles (Figure 2b) were smaller and more uniform than the Fe₃O₄@SiO₂ particles. Also, the EDX analysis of Fe₃O₄@SiO₂ after being modified by VTES (Figure 2e) also showed the Fe, Si, and O elements. The Fe₃O₄@SiO₂@[C4mim]HSO₄ particles (Figure 2c) were more uniform and slightly larger than those before IL modification. Also, the EDX analysis of Fe₃O₄@SiO₂, after being modified by IL (Figure 2f), showed the Fe, Si, and O elements, and the C content was increased significantly. The average diameter of an individual microsphere was calculated to be approximately 0.24 μm. Aggregates were also observed because of adhesion between the magnetic microspheres.

2.2.2. FT-IR Analysis. In Figure 3, the Fe₃O₄@SiO₂ spectra showed a characteristic peak for Fe–O at 560 cm⁻¹ and Si–O

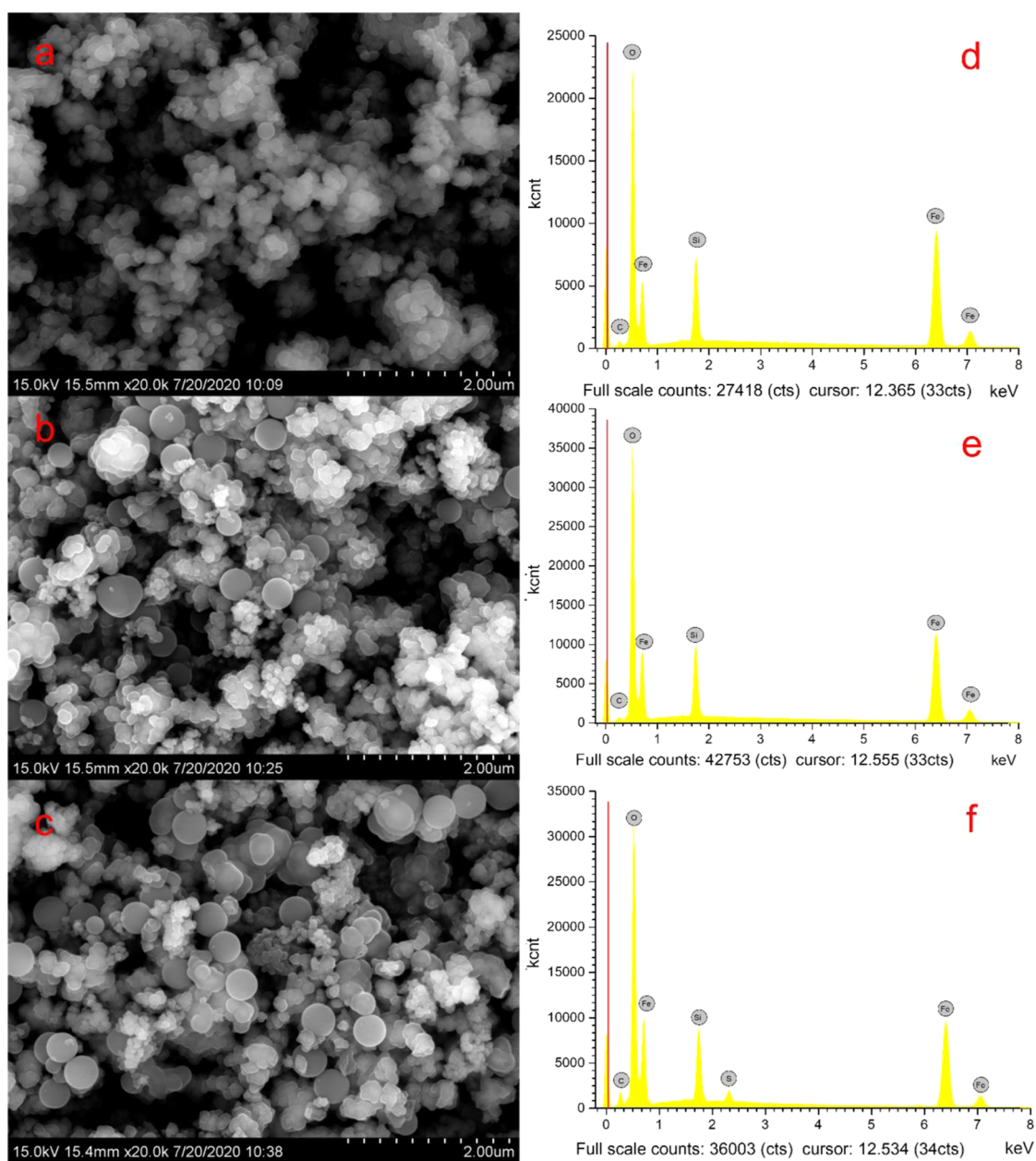


Figure 2. SEM images of $\text{Fe}_3\text{O}_4@SiO_2$ (a), $\text{Fe}_3\text{O}_4@SiO_2@VTES$ (b), and $\text{Fe}_3\text{O}_4@SiO_2@[C4mim]HSO_4$ (c), and mapping analysis of $\text{Fe}_3\text{O}_4@SiO_2$ (d), $\text{Fe}_3\text{O}_4@SiO_2@VTES$ (e), and $\text{Fe}_3\text{O}_4@SiO_2@[C4mim]HSO_4$ (f).

at 1080 cm^{-1} , which proved the existence of Fe_3O_4 . In the infrared spectra of $[C4mim]Br$, a characteristic peak for $C=N$ is observed at 1651 cm^{-1} , that for the butyl group is observed at 1360 cm^{-1} , and the vibration and stretching peaks of the imidazole ring skeleton are observed at 1557 and 1162 cm^{-1} , respectively. In addition, most of the absorption peaks at $500\text{--}1000\text{ cm}^{-1}$ are caused by the flexural vibration of $C-H$ in plane of the ionic liquid. In the infrared spectra of $\text{Fe}_3\text{O}_4@SiO_2@[C4mim]Br$, peaks were observed for bending vibrations of the imidazole ring at 1680 cm^{-1} and for the butyl group at 1360 cm^{-1} , which showed that the ionic liquid was successfully immobilized on the magnetic SiO_2 particles. Peaks at 1581 and 3161 cm^{-1} for the bending and stretching vibrations of OH , respectively, could have been caused by the OH groups on the surface of SiO_2 . An absorption peak near 1068 cm^{-1} was attributed to $Si-O-Si$.

2.2.3. Thermogravimetry-Derivative Thermogravimetry (TG-DTG). TG-DTG curves of $\text{Fe}_3\text{O}_4@SiO_2$ and $\text{Fe}_3\text{O}_4@SiO_2@[C4mim]Br$ were obtained (Figure 4a). When the temperature was increased from room temperature to $600\text{ }^\circ\text{C}$, the mass losses of the two materials were less than 10.0% (4.11% for $\text{Fe}_3\text{O}_4@SiO_2$, 5.27% for $\text{Fe}_3\text{O}_4@SiO_2@VTES$, and 8.67% for $\text{Fe}_3\text{O}_4@SiO_2@[C4mim]Br$). The mass loss is less than 1.5% before heating to $100\text{ }^\circ\text{C}$. There is a significant mass loss peak of $\text{Fe}_3\text{O}_4@SiO_2@[C4mim]Br$ at $350\text{--}400\text{ }^\circ\text{C}$, which indicated the mass loss of the ionic liquid. The TG-DTG curve of $\text{Fe}_3\text{O}_4@SiO_2@[C4mim]Br$ showed three stages of mass loss. The first stage was between 100 and $200\text{ }^\circ\text{C}$, which was caused by the evaporation of solvents with low boiling points. The mass loss for the second stage occurred between 200 and $400\text{ }^\circ\text{C}$, presumably because of the decomposition of a small amount of ionic liquid that was not immobilized on $\text{Fe}_3\text{O}_4@SiO_2$. The third stage occurred between 400 and $600\text{ }^\circ\text{C}$,

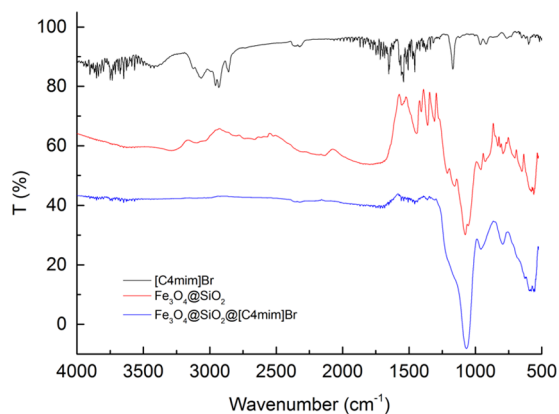


Figure 3. FT-IR analysis of $\text{Fe}_3\text{O}_4@SiO_2$, [C4mim]Br, and $\text{Fe}_3\text{O}_4@SiO_2@[C4mim]Br$.

where slow decomposition or carbonization of the ionic liquid caused the rate of mass loss to slow down. According to the thermogravimetric data, both $\text{Fe}_3\text{O}_4@SiO_2$ and $\text{Fe}_3\text{O}_4@SiO_2@[C4mim]Br$ exhibited good heat resistance. The results for $\text{Fe}_3\text{O}_4@SiO_2@IL$ materials prepared with different ionic liquids are shown in Figure 4b,c; all samples showed good heat resistance.

2.2.4. XRD Analysis. The XRD patterns of $\text{Fe}_3\text{O}_4@SiO_2$ and $\text{Fe}_3\text{O}_4@SiO_2@[C4mim]Br$ (Figure 5a) showed that the samples had strong diffraction peaks at 30.12, 35.54, 37.16, 43.16, 53.68, 57.14, and 62.8° corresponding to the (220), (311), (222), (400), (422), (511), and (440) crystal faces, respectively. These peaks were identical to the characteristic peaks for Fe_3O_4 , and no impurity peaks were present. A broad peak observed at 16–20° was characteristic of silica, indicating successful synthesis of the $\text{Fe}_3\text{O}_4@SiO_2$ particles. In the diffraction curve of $\text{Fe}_3\text{O}_4@SiO_2@IL$, the shapes of peaks were the same as those of $\text{Fe}_3\text{O}_4@SiO_2$, which confirmed that the addition of VTES and ionic liquids cannot change the crystalline form of $\text{Fe}_3\text{O}_4@SiO_2$ particles. The XRD curves for $\text{Fe}_3\text{O}_4@SiO_2@IL$ materials prepared with different ionic liquids are shown in Figure 5b,c.

2.2.5. Brunauer–Emmett–Teller (BET) Analysis. The synthesized $\text{Fe}_3\text{O}_4@SiO_2@VTES$ and magnetic immobilized ionic liquid materials were subjected to pore structure analysis and characterization (Table 4). The specific surface area of the $\text{Fe}_3\text{O}_4@SiO_2@VTES$ particles (51.796 m^2/g) was twofold that of the $\text{Fe}_3\text{O}_4@SiO_2$ particles (23.5897 m^2/g) (Table 4). However, after immobilization of the ionic liquid to prepare $\text{Fe}_3\text{O}_4@SiO_2@IL$, the specific surface area decreased obviously, which could be attributed to an increase in the particle size. For the materials prepared from different ionic liquids, the specific surface areas of $\text{Fe}_3\text{O}_4@SiO_2@[C4mim]Br$ (10.8417 m^2/g) and $\text{Fe}_3\text{O}_4@SiO_2@[C4mim]Ac$ (10.4181 m^2/g) were larger than those of $\text{Fe}_3\text{O}_4@SiO_2@[C4mim]HSO_4$ (10.1231 m^2/g) and $\text{Fe}_3\text{O}_4@SiO_2@[C4mim]OH$ (9.1289 m^2/g). $\text{Fe}_3\text{O}_4@SiO_2@[C4mim]NO_3$ had the lowest specific surface area (4.7786 m^2/g). Although some channels of the catalyst are blocked by ionic liquids, the catalytic sites are increased and the adsorption of biodiesel is reduced.

The pore size distributions (Figure 6) showed that $\text{Fe}_3\text{O}_4@SiO_2$ had concentrated peaks at 3–5, 11, and 40 nm, indicating that the particles contained pores of multiple sizes. After modification with VTES to prepare $\text{Fe}_3\text{O}_4@SiO_2@VTES$ particles, the pore size increased and peaks were observed at

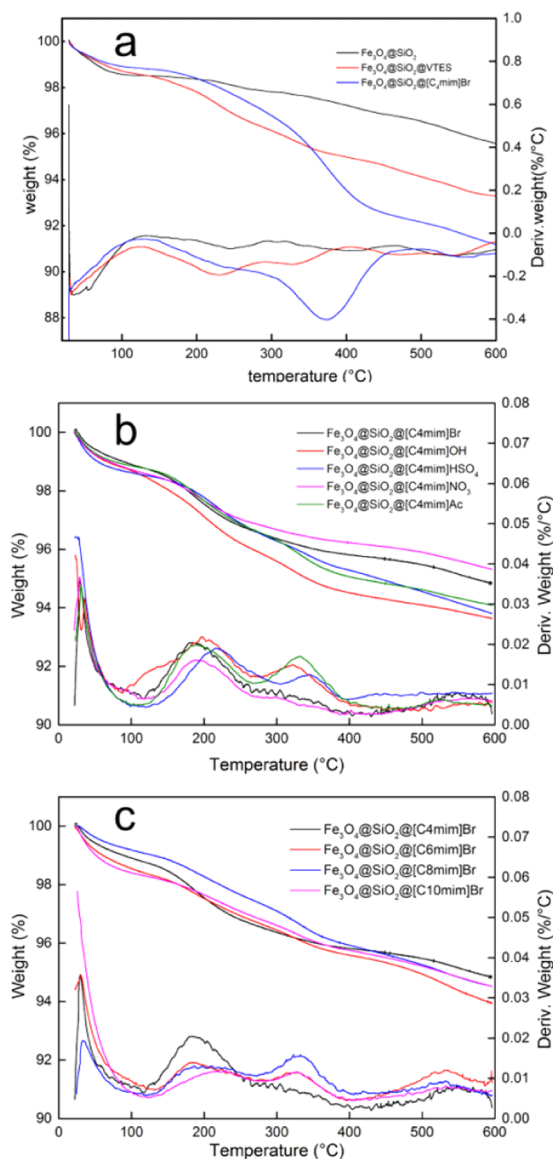


Figure 4. TG and DTG curves of $\text{Fe}_3\text{O}_4@SiO_2$, $\text{Fe}_3\text{O}_4@SiO_2@VTES$, and $\text{Fe}_3\text{O}_4@SiO_2@[C4mim]IL$, (a) TG and DTG curves of $\text{Fe}_3\text{O}_4@SiO_2$, $\text{Fe}_3\text{O}_4@SiO_2@VTES$, and $\text{Fe}_3\text{O}_4@SiO_2@[C4mim]Br$, (b) TG and DTG curves of $\text{Fe}_3\text{O}_4@SiO_2@[C4mim]Br$, $\text{Fe}_3\text{O}_4@SiO_2@[C4mim]OH$, $\text{Fe}_3\text{O}_4@SiO_2@[C4mim]HSO_4$, $\text{Fe}_3\text{O}_4@SiO_2@[C4mim]NO_3$, and $\text{Fe}_3\text{O}_4@SiO_2@[C4mim]Ac$, and (c) TG and DTG curves of $\text{Fe}_3\text{O}_4@SiO_2@[C4mim]Br$, $\text{Fe}_3\text{O}_4@SiO_2@[C6mim]Br$, $\text{Fe}_3\text{O}_4@SiO_2@[C8mim]Br$, and $\text{Fe}_3\text{O}_4@SiO_2@[C10mim]Br$.

3–5, 25, and 40 nm (Figure 6a). These results show that the modified magnetic SiO_2 particles have more binding sites for the ionic liquid than the nonmodified particles, which greatly enhance the adsorption quantity. When the ionic liquid [C4mim]Br was immobilized, the number of pores (below 20 nm) is not changed, while the number of pores (greater than 30 nm) is decreased. This could be caused by excessive ionic liquid filling in the larger pores. The pore size distributions of the $\text{Fe}_3\text{O}_4@SiO_2@IL$ particles prepared with different ionic liquids are shown in Figure 6b,c.

2.3. Single-Factor Analysis of Catalysts and Biodiesel Preparation. **2.3.1. Screening of Different Magnetic Immobilized Ionic Liquid Catalysts.** Suitable catalytic conditions (i.e., reaction time of 3 h and volume ratio of

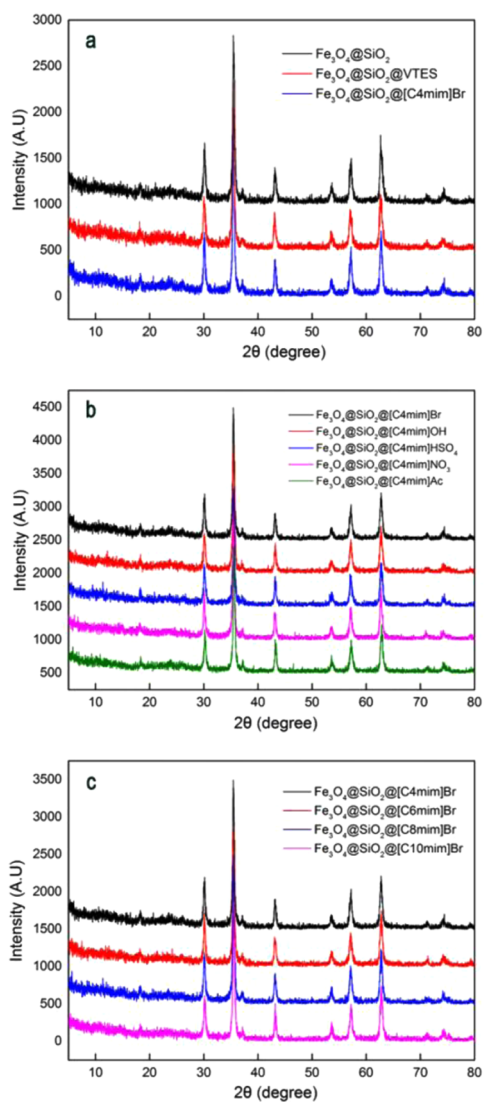


Figure 5. XRD analysis of $\text{Fe}_3\text{O}_4@SiO_2$, $\text{Fe}_3\text{O}_4@SiO_2@VTES$, and $\text{Fe}_3\text{O}_4@SiO_2@[C4mim]IL$. (a) XRD analysis of $\text{Fe}_3\text{O}_4@SiO_2$, $\text{Fe}_3\text{O}_4@SiO_2@VTES$, and $\text{Fe}_3\text{O}_4@SiO_2@[C4mim]Br$, (b) XRD analysis of $\text{Fe}_3\text{O}_4@SiO_2@[C4mim]Br$, $\text{Fe}_3\text{O}_4@SiO_2@[C4mim]OH$, $\text{Fe}_3\text{O}_4@SiO_2@[C4mim]HSO_4$, $\text{Fe}_3\text{O}_4@SiO_2@[C4mim]NO_3$, and $\text{Fe}_3\text{O}_4@SiO_2@[C4mim]Ac$, and (c) XRD analysis of $\text{Fe}_3\text{O}_4@SiO_2@[C4mim]Br$, $\text{Fe}_3\text{O}_4@SiO_2@[C6mim]Br$, $\text{Fe}_3\text{O}_4@SiO_2@[C8mim]Br$, and $\text{Fe}_3\text{O}_4@SiO_2@[C10mim]Br$.

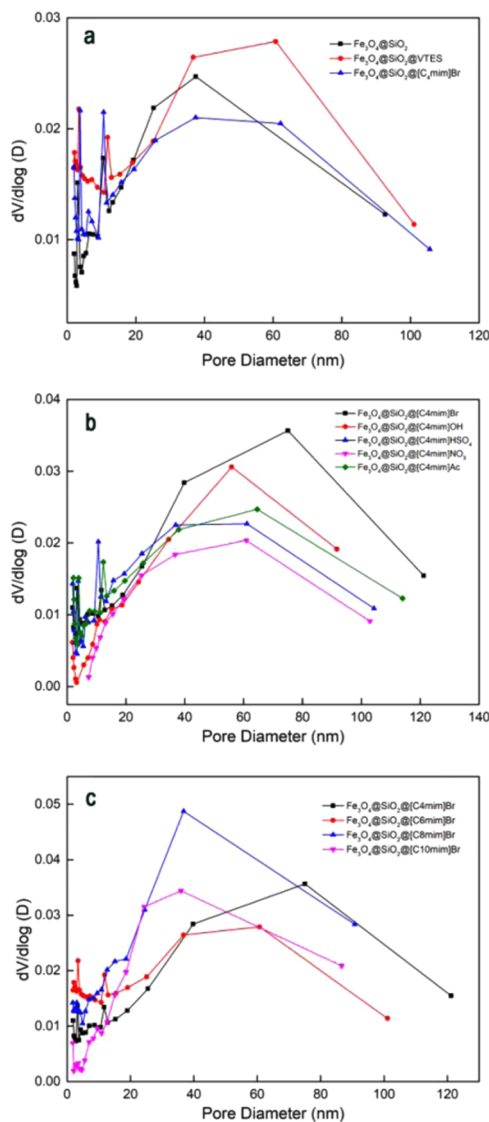


Figure 6. Pore size distributions of $\text{Fe}_3\text{O}_4@SiO_2$, $\text{Fe}_3\text{O}_4@SiO_2@VTES$, and $\text{Fe}_3\text{O}_4@SiO_2@[C4mim]IL$. (a) Pore size distributions of $\text{Fe}_3\text{O}_4@SiO_2$, $\text{Fe}_3\text{O}_4@SiO_2@VTES$, and $\text{Fe}_3\text{O}_4@SiO_2@[C4mim]Br$. (b) Pore size distributions of $\text{Fe}_3\text{O}_4@SiO_2@[C4mim]Br$, $\text{Fe}_3\text{O}_4@SiO_2@[C4mim]OH$, $\text{Fe}_3\text{O}_4@SiO_2@[C4mim]HSO_4$, $\text{Fe}_3\text{O}_4@SiO_2@[C4mim]NO_3$, and $\text{Fe}_3\text{O}_4@SiO_2@[C4mim]Ac$. (c) Pore size distributions of $\text{Fe}_3\text{O}_4@SiO_2@[C4mim]Br$, $\text{Fe}_3\text{O}_4@SiO_2@[C6mim]Br$, $\text{Fe}_3\text{O}_4@SiO_2@[C8mim]Br$, and $\text{Fe}_3\text{O}_4@SiO_2@[C10mim]Br$.

Table 4. Pore Size of Synthetic Ionic Liquids Immobilized in a Magnetic Catalyst

no.	name	specific surface area of BET (m^2/g)	pore volume (cm^3/g)	average pore size (nm)
1	$\text{Fe}_3\text{O}_4@SiO_2$ (250 rpm)	9.2260	0.0234	3.9684
2	$\text{Fe}_3\text{O}_4@SiO_2$ (350 rpm)	23.5897	0.0424	3.2740
3	$\text{Fe}_3\text{O}_4@SiO_2@VTES$	51.7960	0.0155	6.7038
4	$\text{Fe}_3\text{O}_4@SiO_2@[C4mim]HSO_4$	10.1231	0.0169	6.6855
5	$\text{Fe}_3\text{O}_4@SiO_2@[C4mim]NO_3$	4.7786	0.0090	7.5459
6	$\text{Fe}_3\text{O}_4@SiO_2@[C4mim]OH$	9.1289	0.0153	6.7256
7	$\text{Fe}_3\text{O}_4@SiO_2@[C4mim]Ac$	10.4181	0.0179	6.8632
8	$\text{Fe}_3\text{O}_4@SiO_2@[C4mim]Br$	10.8417	0.0203	6.5074
9	$\text{Fe}_3\text{O}_4@SiO_2@[C6mim]Br$	16.2261	0.0262	6.4516
10	$\text{Fe}_3\text{O}_4@SiO_2@[C8mim]Br$	19.9035	0.0351	7.0634
11	$\text{Fe}_3\text{O}_4@SiO_2@[C10mim]Br$	22.3239	0.0498	8.4169

Table 5. Biodiesel Synthesis with Different Types of Catalysts

no.	type	catalysts	acidity/alkalinity	biodiesel yield (g/10.00 g)
1	inorganic acid	H ₂ SO ₄	acidic	5.21
2	gel-ion exchange resin	001*7	acidic	4.19
3	ionic liquid	[C4mim]HSO ₄	acidic	5.50
4	immobilized ionic liquid	Fe ₃ O ₄ @SiO ₂ @[C4mim]HSO ₄	acidic	5.57
5	immobilized ionic liquid	Fe ₃ O ₄ @SiO ₂ @[C4mim]CH ₃ SO ₃	acidic	5.36
6	immobilized ionic liquid	Fe ₃ O ₄ @SiO ₂ @[C4mim]NO ₃	acidic	5.50
7	inorganic base	NaOH	alkaline	4.35
8	immobilized ionic liquid	Fe ₃ O ₄ @SiO ₂ @[C4mim]OH	alkaline	5.15
9	immobilized ionic liquid	Fe ₃ O ₄ @SiO ₂ @[C4mim]Ac	alkaline	5.03
10	immobilized ionic liquid	Fe ₃ O ₄ @SiO ₂ @[C4mim]Br	neutral	0.15

7:1) from the initial experiments were used with 1.50 g of the catalyst for methyl esterification under reflux. Different immobilized ionic liquid catalysts were investigated, and the biodiesel yields were evaluated to select the optimum catalyst (Table 5). 001*7 gel-ion exchange resin and ionic liquid-[C4mim]HSO₄ were used as catalysts for comparison. Among the catalysts, Fe₃O₄@SiO₂@[C4mim]HSO₄ had the best catalytic effect and gave a biodiesel yield of 5.57/10.00 g (biodiesel/seed oil), a little higher than catalysis by [C4mim]-NO₃ (5.50/10.00 g). The catalytic efficiency of the acidic immobilized ionic liquid catalyst was better than that of the alkaline catalyst because saponification and side reactions occurred with the alkaline catalyst, which reduced the biodiesel yield. By contrast, immobilized ionic liquids without acid–base sites did not catalyze the esterification reaction.

2.3.2. Single-Factor Analysis of Biodiesel Preparation. Single-factor analysis of the esterification reaction was carried out for the biodiesel preparation to investigate the reaction time, volume ratio of methanol to seed oil, and the weight of the catalyst. The biodiesel was prepared by catalytic synthesis with Fe₃O₄@SiO₂@[C4mim]HSO₄.

To investigate the reaction time, the mixture was heated to reflux for 1, 2, 3, 4, or 5 h. The synthetic biodiesel greatly increased when the reaction time was increased from 1 to 3 h and then only slightly increased with further increase above 3 h (Figure 7a). These results indicate that the reaction is close to completion at 3 h. The small increase in the yield obtained when increasing the reaction time beyond 3 h would not be worth the increase in energy requirements. Therefore, 3 h was selected as the optimum reaction time for biodiesel preparation.

To investigate the effect of the volume ratio of methanol to seed oil, we used the procedure described above with 10.0 g of seed oil, a reaction time of 3 h, 1.50 g of the catalyst, and volume ratios of 5:1, 6:1, 7:1, 8:1, and 9:1. For volume ratios above 7:1, the yield of biodiesel was almost constant, which indicated that methanol volume seven times that of seed oil was sufficient for the reaction (Figure 7b). Considering the cost of methanol recovery in industrial production, a methanol to seed oil volume ratio of 7:1 was selected as the optimum ratio.

To investigate the effect of the dosage of the catalyst, we used a reaction time of 3 h and a methanol to seed oil volume ratio of 7:1. The yield of biodiesel greatly increased when the mass of the catalyst was increased from 0.50 to 1.50 g; when the mass of the catalyst was more than 1.50 g, the yield of biodiesel increased slightly, and 1.50 g of the magnetic immobilized ionic liquid catalyst was selected as the optimum dosage (Figure 7c).

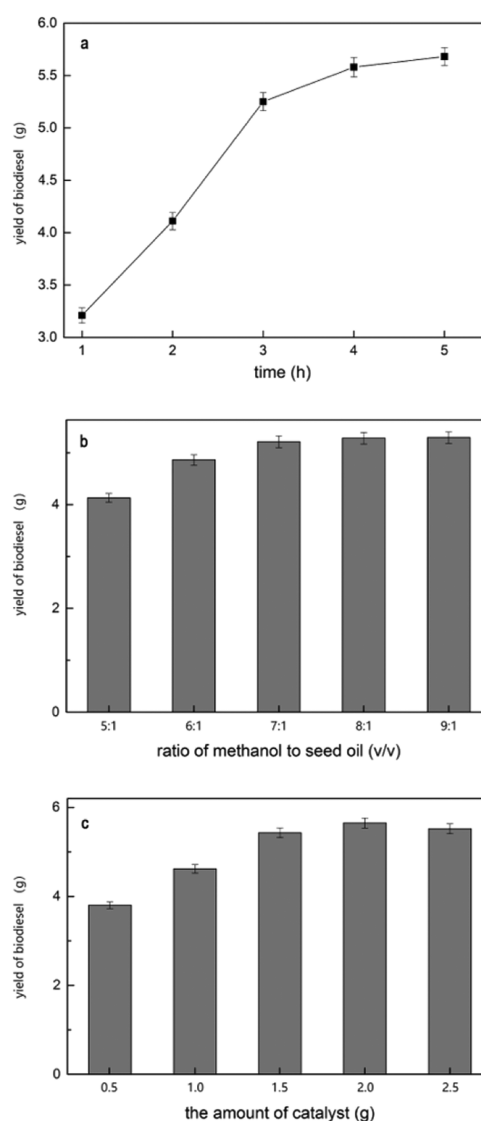


Figure 7. Single-factor analysis for biodiesel preparation. (a) Effect of the reaction time on the biodiesel yield. (b) Effect of the methanol volume on the biodiesel yield. (c) Effect of the catalyst dosage on the biodiesel yield.

The above experiments were repeated three times, and the results were averaged.

2.3.3. Determination of *S. chinensis* Seed Oil and Biodiesel Chemical Indicators. The acid value, iodine value, saponification value, and peroxide value of the seed oil and biodiesel were determined under the optimum catalytic

Table 6. Chemical Indexes of Seed Oil and Biodiesel

no.	name	catalysts	acid/alkaline	acid value (mg KOH/g)	iodine value (mg KI/g)	saponification value (mg KOH/g)	peroxide value (mg/100 g)
1	seed oil			11.5	107.8	108.8	0.25
2	biodiesel	H ₂ SO ₄	acid	5.6	66.4	78.4	0.63
3	biodiesel	001*7	acid	5.6	48.2	58.1	1.52
4	biodiesel	[C4mim]HSO ₄	acid	6.4	68.7	86.6	1.52
5	biodiesel	Fe ₃ O ₄ @SiO ₂ @[C4mim]HSO ₄	acid	5.4	66.5	78.5	0.63
6	biodiesel	Fe ₃ O ₄ @SiO ₂ @[C4mim]NO ₃	acid	5.4	52.0	70.7	0.36
7	biodiesel	Fe ₃ O ₄ @SiO ₂ @[C4mim]OH	alkaline	3.5	70.1	89.6	0.38
8	biodiesel	Fe ₃ O ₄ @SiO ₂ @[C4mim]Ac	alkaline	4.6	70.4	89.7	0.75

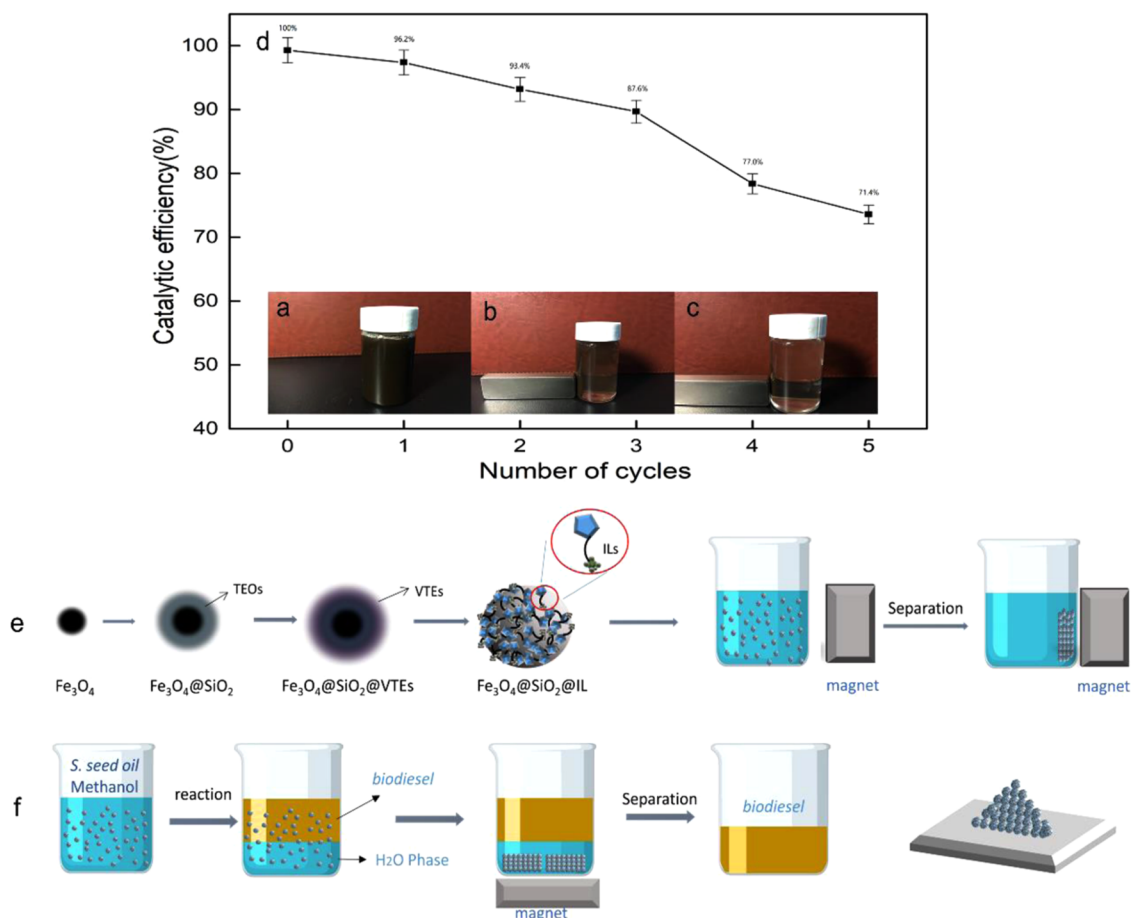


Figure 8. Recycling of the magnetic immobilized ionic liquid materials. (a)–(c) Photographs of recycling of the magnetic immobilized ionic liquid materials. (d) Catalytic efficiency after recycling of the magnetic immobilized ionic liquid materials. (e) Preparation of the magnetic immobilized ionic liquid materials. (f) Application of the magnetic immobilized ionic liquid materials. Photograph courtesy of ‘Yinhang Wang’. Copyright 2021, and the image is free domain.

conditions (Table 6). The experimental results showed that the acid value, iodine value, and saponification value of biodiesel were lower than those of seed oil, whereas the peroxide value was much higher than that of seed oil. These results showed that the catalytic reaction was complete and that the quantities of fatty acids and free acids decreased with the conversion from seed oil to biodiesel. At the same time, the decrease in the iodine value showed that the degree of unsaturation decreased. The results also indicated that the product had a higher esterification efficiency than the starting material. The acid value of biodiesel with the acidic catalyst

[C4mim]HSO₄ is the highest. Also, the acid value of biodiesel with the basic catalyst is lower. [C4mim]Ac is a weak base ionic liquid, and Ac⁻ in the ionic liquid is different from Ac⁻ in NaAc. As NaAc is a weak acid, strong base salt, the ionization of NaAc is greater than the hydrolysis of Ac⁻. However, in ionic liquid, the cation is an imidazole ring with an alkyl chain; the ionization of [C4mim]Ac is negligible. Thus, the hydrolysis of Ac⁻ is the main resource of OH⁻. Also, the hydrolysis of Ac⁻ is a reversible reaction. If the acid of seed oil is less, the alkalinity of [C4mim]Ac is even weaker. The alkalinity of [C4mim]OH is much stronger than the alkalinity of

[C4mim]Ac. Therefore, the acid value of the biodiesel with the alkaline catalyst $\text{Fe}_3\text{O}_4@\text{SiO}_2@[\text{C4mim}]\text{Ac}$ is a little higher than that with the alkaline catalyst $\text{Fe}_3\text{O}_4@\text{SiO}_2@[\text{C4mim}]\text{-OH}$.

2.4. Recycling of the Magnetic Immobilized Ionic Liquid Catalyst. After each experiment, the magnetic immobilized ionic liquid catalyst was recovered and reused. The solid phase was separated from the reaction mixture by a magnetic field, washed repeatedly with ethanol and deionized water ultrasonically, and then vacuum dried at room temperature. After four cycles of recovery and reuse, the catalytic efficiency of $\text{Fe}_3\text{O}_4@\text{SiO}_2@[\text{C4mim}]\text{HSO}_4$ was 87.6% of the initial catalytic activity; after six cycles of recovery and reuse, the catalytic efficiency of $\text{Fe}_3\text{O}_4@\text{SiO}_2@[\text{C4mim}]\text{-HSO}_4$ was 71.4% of the initial catalytic activity (Figure 8). The biodiesel yield might have decreased because of traces of glycerol that interact with the anion of IL through possible hydrogen bonding, or the acid sites covered on the support surface, which fell off easily from the surface, which causes a decrease in its efficiency for catalytic transesterification.

2.5. Thermal Gravimetric Analysis of *S. chinensis* Seed Oil and Biodiesel. TG-DTG curves were obtained for *S. chinensis* seed oil and biodiesel (Figure 9). Under nitrogen

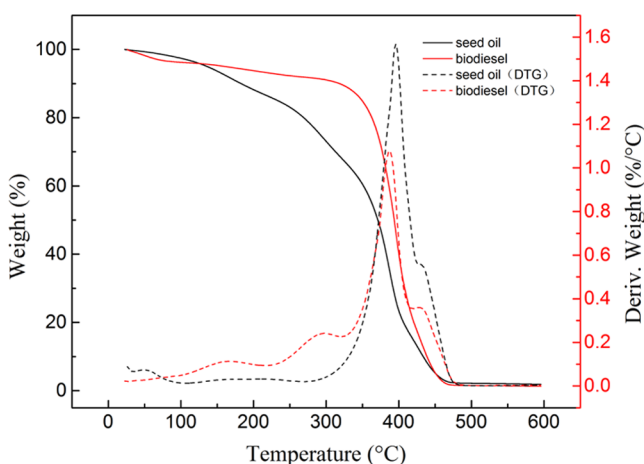


Figure 9. TG and DTG curves of seed oil and biodiesel.

protection, the temperature was increased at 10 °C/min, and scanning was performed at 50–600 °C to measure the mass loss of each sample and examine its thermal stability. A gradual mass loss of the seed oil was observed from 100 to 450 °C. There were two obvious stages of the seed oil mass loss (100–300, 300–450 °C). The first stage was between 100 and 300 °C, which was caused by fatty acids with low molecular weights and combustion points. The mass loss for the second stage occurred between 300 and 450 °C, presumably because of the decomposition of the long chains in seed oil. The results indicated that the seed oil contained impurities, had a wide combustion temperature range, and an unstable ignition point. There was one obvious stage of the biodiesel mass loss for fatty acid esters (300–450 °C). The results indicated that the biodiesel was more heat stable than seed oil, it had a more uniform composition, and contained fewer impurities. Biodiesel was much more suitable for use as an engine fuel than seed oil.

2.6. FT-IR Analysis of *S. chinensis* Seed Oil and Biodiesel. FT-IR results for the biodiesels prepared from *S. chinensis* seed oil with different catalysts are shown in Figure

10. In the spectra of both seed oil and biodiesel, a strong absorption peak was observed at 1460–1050 cm^{-1} , and peaks

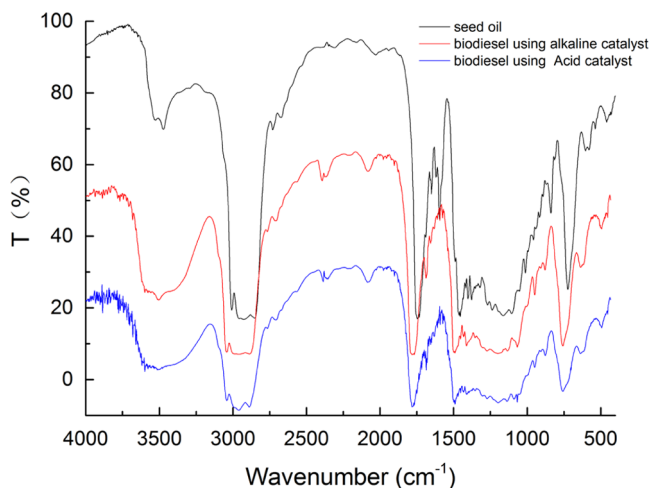


Figure 10. FT-IR analysis of seed oil and biodiesel.

for alkyl CH were observed at 2926 and 2855 cm^{-1} . Peaks that could be attributed to the breaking of ester bonds in biodiesel and seed oil were present at 1710–1550 cm^{-1} for the carboxylic acid C=O bond and 3600 cm^{-1} for the carboxyl. These peaks were produced by free carboxylic acid and other impurities. Characteristic peaks for the methoxy were observed at 850 and 1017 cm^{-1} . These results indicated that the samples contained fatty acid methyl esters.

2.7. Composition of *S. chinensis* Seed Oil and Biodiesel. GC-MS is a quick and easy method for determining the chemical composition. It can be used to quantitatively determine if fatty acid methyl esters are the main components of biodiesel. In this study, GC-MS was used to analyze the chemical compositions of biodiesels prepared from *S. chinensis* seed oil with different catalysts. The seed oil was composed of 28.33% C16 fatty acid, 67.77% C18 fatty acid, and 78.45% unsaturated fatty acid. Table 7 shows the compositions of biodiesels prepared with different acid–base catalysts. Among the components of biodiesel produced by $\text{Fe}_3\text{O}_4@\text{SiO}_2@[\text{C4mim}]\text{HSO}_4$, methyl linoleate (C18:2, 48.69%) had the highest proportion among these ingredients, followed by methyl oleate (C18:1, 9.50%) and alkalinity methyl palmitate (C16:0, 7.31%). Quantitative analysis can be used to determine whether the esterification reaction with an acidic ionic liquid catalyst is more complete than the one with a basic catalyst. The GC-MS spectra and composition data of seed oil and biodiesel are shown in the Supporting Information Figures S1, S2, and Tables S1, S2.

2.8. Calorific Value of *S. chinensis* Seed Oil and Biodiesel. The heat of combustion of the biodiesel was measured by oxygen bomb calorimetry XRY-1A using the ASTM D240 method,²¹ and each sample was run three times and averaged. The standard deviation between measurements was never more than 0.15 and the coefficient of variance was not greater than 0.5%, indicating a high degree of precision in our experimental technique. The gross (H_c) and net (H_n) heats of combustion for seed oil and biodiesel are shown in Table 8. The highest net heat of *S. chinensis* seed oil was only 32.14 kJ/g, and the biodiesel catalyzed by $\text{Fe}_3\text{O}_4@\text{SiO}_2@[\text{C4mim}]\text{HSO}_4$ was 38.28 kJ/g, while the biodiesel catalyzed by other $\text{Fe}_3\text{O}_4@\text{SiO}_2@[\text{ILs}]$ had the highest net heat

Table 7. Chemical Analysis of Biodiesel

no.	catalysts	acid/alkaline	alkalinity methyl palmitate C16:0 (%)	methyl stearate C18:0 (%)	methyl oleate C18:1 (%)	methyl linoleate C18:2 (%)	methyl linolenic acid C18:3 (%)
1	Fe ₃ O ₄ @SiO ₂ @ [C4mim]HSO ₄	acidity	7.31	1.47	9.50	48.69	0.56
2	Fe ₃ O ₄ @SiO ₂ @ [C4mim]NO ₃	acidity	6.32	1.23	9.64	38.02	0.77
3	Fe ₃ O ₄ @SiO ₂ @ [C4mim]Ac	alkaline	4.03	1.34	1.44	24.30	0.61
4	Fe ₃ O ₄ @SiO ₂ @ [C4mim]OH	alkaline	6.17	1.14	8.75	26.99	0.61

Table 8. Experimental Gross (H_c) and Net (H_n) Heat of Combustion Data of Seed Oil and Biodiesel

sample	catalyst	H _c (kJ/g)	H _n (kJ/g)
seed oil		32.14	30.62
biodiesel	Fe ₃ O ₄ @SiO ₂ @ [C4mim]HSO ₄	38.28	36.58
biodiesel	Fe ₃ O ₄ @SiO ₂ @ [C4mim]NO ₃	37.66	35.40
biodiesel	Fe ₃ O ₄ @SiO ₂ @ [C4mim]OH	37.22	35.18
biodiesel	Fe ₃ O ₄ @SiO ₂ @ [C4mim]Ac	36.13	33.51

were 37.66 kJ/g for Fe₃O₄@SiO₂@ [C4mim]NO₃, 37.22 kJ/g for Fe₃O₄@SiO₂@ [C4mim]OH, and 36.13 kJ/g for Fe₃O₄@SiO₂@ [C4mim]Ac. The calorific value is an important parameter in the selection of a fuel. The calorific value of biodiesel is usually lower than that of diesel due to its higher oxygen content.²⁰ Although the heating value of *S. chinensis* biodiesel was lower than diesel of the national standard (about 42.00 kJ/g), the increase was still quite significant from the heating value of *S. chinensis* seed oil. Also, in future studies, the novel magnetic catalyst immobilized with other types of ionic liquids would be developed for the catalytic synthesis of biodiesel.

2.9. Catalytic Mechanisms with Fe₃O₄@SiO₂@ [C4mim]HSO₄. Figure 11 shows the proposed catalytic mechanism of Fe₃O₄@SiO₂@ [C4mim]HSO₄ with methanol. Ionic liquid [C4mim]HSO₄ was applied as a catalyst for the catalytic esterification reaction of fatty acid from seed oil. The

proposed esterification mechanism is shown in Figure 11b. Also, the reaction process can be divided into two main processes: protonation and dehydration.

First, H⁺ produced by the hydrolysis of HSO₄⁻ anion binds to carbon-based atoms in the carboxylic acid molecules, making the carbon atom of the carboxyl group more electrophilic, which is beneficial to the attack of oxygen atom in the alcohol hydroxyl group to form a new carbon–oxygen bond. In addition, H⁺ attached to the hydroxyl oxygen from the intermediate to form an oxonium salt, as shown in Figure 11a. A positively polarized—OH hydrogen atom from an alcoholic molecule is attracted to a lone pair of electrons on a negatively polarized oxygen atom of a carbonyl molecule. Second, any one of the hydroxyl is protonated and released a molecule of water, and then the carboxylic acid ester was formed, while a proton is lost from the other hydroxyl as shown in Figure 11c. A similar reaction mechanism of biodiesel synthesis has been reported for different catalysts by various researchers.²²

3. CONCLUSIONS

A magnetic immobilized ionic liquid catalyst was synthesized by immobilizing an ionic liquid on modified magnetic SiO₂ particles. SEM showed that the magnetic immobilized ionic liquid catalyst particles were spherical, with an average particle diameter of about 240 nm. FT-IR analysis showed that the magnetic immobilized ionic liquids had characteristic absorp-

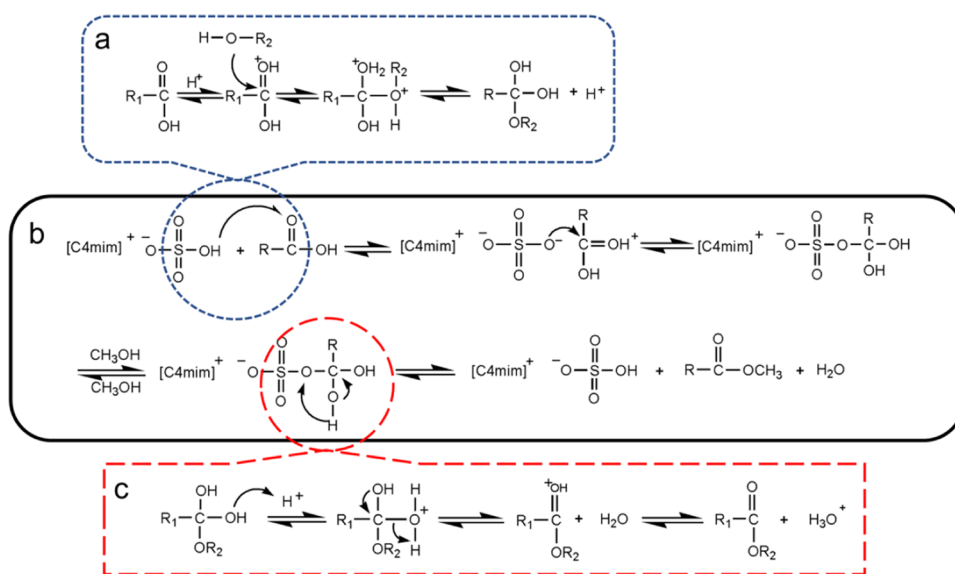
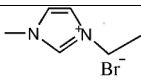
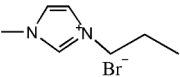
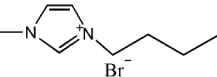
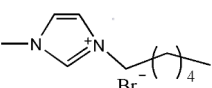
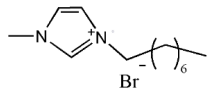
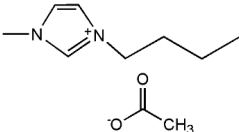
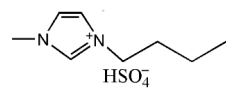
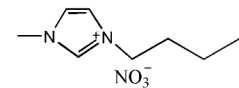
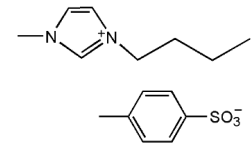


Figure 11. Catalytic mechanisms with Fe₃O₄@SiO₂@ [C4mim]HSO₄. (a) Catalytic mechanisms with the interaction of proton with the carbonyl. (b) Overview of the whole reaction mechanism of Fe₃O₄@SiO₂@ [C4mim]HSO₄-catalyzed esterification of seed oil. (c) Catalytic mechanisms with deprotonation of an oxonium ion.

Table 9. Experimental Ionic Liquids

Name	Molecular formula	Molecular weight	State (room temperature)	Purity	Structural formula
1-ethyl-3-methylimidazolium bromide	[C2mim]Br	191.07	liquid	99%	
1-propyl-3-methylimidazolium bromide	[C3mim]Br	202.1	liquid	99%	
1-butyl-3-methylimidazolium bromide	[C4mim]Br	219.20	liquid	99%	
1-hexyl-3-methylimidazolium bromide	[C6mim]Br	247.18	liquid	99%	
1-octyl-3-methylimidazolium bromide	[C8mim]Br	275.23	liquid	99%	
1-butyl-3-methylimidazolium acetate	[C4mim]Ac	198.26	liquid	99%	
1-butyl-3-methylimidazolium hydrogen sulfate	[C4mim]HSO ₄	236.29	solid	97%	
1-butyl-3-methylimidazolium nitrate	[C4mim]NO ₃	201.22	liquid	99%	
1-butyl-3-methylimidazole p-toluenesulfonate	[C4mim]CH ₂ -C ₆ H ₄ -HSO ₃	310.41	solid	99%	

tion peaks for Fe₃O₄ and imidazole rings. XRD results showed that the process of immobilizing the ionic liquids did not damage the crystal structure of magnetic silica. The optimum synthesis conditions were a stirring speed of 350 rpm and a TEOS volume of 5.0 mL in the first step, a VTES amount of 10.0 mmol and a reaction time of 12 h in the second step, and an ionic liquid amount of 10.0 mmol. The average loading of Fe₃O₄@SiO₂@[C4mim]OH was 206.83 ± 12.13 mg/g, and more than 43.63% of the ionic liquid was successfully supported on the magnetic SiO₂ particles. Catalysts with different ionic liquids were prepared under the optimum

conditions. The catalytic efficiency was 87.6% after four repeated recovery and reuse experiments, indicating that the catalyst has stable catalytic performance and good recyclability.

The optimum conditions for the preparation of biodiesel from *S. chinensis* seed oil were a methylation reaction time of 3 h, a volume ratio of methanol to seed oil (v/v) of 7:1, and 1.50 g of catalyst. The catalytic efficiency of Fe₃O₄@SiO₂@[C4mim]HSO₄ was relatively high, and the yield of biodiesel was 5.57/10.00 g. The chemical indexes of seed oil and biodiesel were determined. The catalytic effect of the acidic catalyst was better than that of the alkaline catalyst, which

would result in saponification. TG analysis showed that the pyrolysis temperature of biodiesel was lower than that of seed oil. Because of its uniform composition and good combustion performance (the highest net heat of the biodiesel catalyzed by $\text{Fe}_3\text{O}_4@\text{SiO}_2@[\text{C4mim}]\text{HSO}_4$ was 38.28 kJ/g), biodiesel is more suitable as a fuel. Furthermore, the catalytic mechanisms with $\text{Fe}_3\text{O}_4@\text{SiO}_2@[\text{C4mim}]\text{HSO}_4$ were interpreted.

4. MATERIAL AND METHODS

4.1. Materials and Reagents. **4.1.1. Materials.** The fruit of *S. chinensis* (Turcz.) Baill were purchased from the Sankeshu Medicinal Materials Market (Harbin, China) and were air-dried at room temperature in a shady and ventilated place. The fruit were harvested in the Northeast Xing'anling area of China in September 2017.

4.1.2. Chemical Reagents. All ionic liquids used in this work (Table 9) were purchased from the Cheng Jie Chemical Co., Ltd. (Shanghai, China). High-performance liquid chromatography (HPLC)-grade methanol and acetic acid were purchased from J&K Chemical, Ltd. (Beijing, China). Deionized water for use in the experimental work was obtained using a Milli-Q water purification system (Millipore, Billerica, MA). Petroleum ether, absolute ethanol, and trichloromethane were purchased from the Fu Yu Chemical Co., Ltd. (Tianjin, China). The other solvents and chemicals used in this study were of analytical grade and were purchased from the Beijing Chemical Reagents Co. (Beijing, China). All solutions used for HPLC were prefiltered through 0.45- μm membranes (Guangfu Chemical Reagents Co., Tianjin, China) before use.

4.2. Methods. **4.2.1. Preparation of the Magnetic Immobilized Ionic Liquid Catalyst.** First, 1.50 g of Fe_3O_4 particles were mixed with absolute ethanol (400 mL) under sonication (Kunshan Ultrasonic Instruments Co., Ltd.) for 10 min until the particles were distributed uniformly in the solvent. Water (60 mL), aqueous ammonia (30 mL; the mass fraction of ammonia in the aqueous solution is 25%), and a certain volume of tetraethyl orthosilicate (TEOS) were added sequentially to the mixture and the reaction was allowed to proceed for 5 h at 25 °C under continuous mechanical stirring. The product was separated and collected with a magnet, followed by washing sequentially with ethanol and water three times with each solvent. The obtained product was dried in a vacuum oven at 25 °C for 24 h.

Next, the $\text{Fe}_3\text{O}_4@\text{SiO}_2$ particles (3.00 g) were mixed with a certain amount of vinyltriethoxysilane (VTES). An excess of triethylamine (about 40 mL) was added to the mixture as a reflux solvent and catalyst. The reaction was heated to reflux and stirred under reflux for 12 h. The obtained product ($\text{Fe}_3\text{O}_4@\text{SiO}_2@VTES$) was repeatedly washed with methanol to remove impurities and then dried in a vacuum oven at 40 °C for 24 h.

Finally, the $\text{Fe}_3\text{O}_4@\text{SiO}_2@VTES$ particles (3.00 g) were mixed with 0.04 g of the fat-soluble initiator Azobisisobutyronitrile (AIBN) and different kinds of ionic liquids. Chloroform (35 mL) was added to the mixture, and the reaction was allowed to proceed for 1 h at 25 °C under continuous mechanical stirring. The mixture was then heated to 75 °C to remove chloroform, followed by heating to 100 °C for 2 h to obtain the magnetic immobilized ionic liquid ($\text{Fe}_3\text{O}_4@\text{SiO}_2@IL$). This product was washed repeatedly with ethanol and water. The solid phase was separated under an external magnetic field and then dried in a vacuum oven at 40 °C for 24 h.

4.2.2. Characterization of the Magnetic Immobilized Ionic Liquid Catalyst. Scanning electron microscopy (SEM) analysis images with energy-dispersive X-ray spectroscopy (EDX) were recorded on an XL30 electron microscope (Philips, The Netherlands) operated at 10.0 kV. A thin gold film was sprayed on each sample before analysis. XRD patterns were recorded on a D/MAX2200 X-ray diffractometer (Limited company Co. Aichi Shibuya, Japan) using $\text{Cu K}\alpha$ radiation. Nitrogen sorption isotherms were measured at 77 K with a Micrometrics Tristar 3000 analyzer. Before analysis, the samples were degassed under vacuum at 200 °C for more than 5 h. The Brunauer–Emmett–Teller method was utilized to calculate the specific surface areas. The Barrett–Joyner–Halenda model was used to derive the pore volumes and pore size distributions from the desorption branches of the isotherms. The total pore volumes were estimated from the quantities adsorbed at a relative pressure (P/P_0) of 0.992.

4.2.3. Preparation of *S. chinensis* Seed Oil. *S. chinensis* fruit (10.00 g) was added to a round-bottom flask charged with a certain volume of petroleum ether, and heated under reflux for 2.5 h. The organic phase was separated by a filter and then evaporated under vacuum until a light-yellow viscous liquid remained. The petroleum ether was completely volatilized at 60 °C for 4 h. The resulting *S. chinensis* seed oil was weighed for the preparation of biodiesel.

4.2.4. Preparation of Biodiesel. About 10.00 g of *S. chinensis* seed oil was accurately weighed into a three-neck flask. Anhydrous methanol was added to the flask with a volume ratio of methanol to seed oil (5:1, 6:1, 7:1, 8:1, and 9:1 v/v). Then, the magnetic immobilized ionic liquid catalyst was added. The mixture was then heated under reflux for a certain time. After the esterification reaction was complete, the cooled solution was separated by stratification and the solid catalyst was separated under an external magnetic field. After the esterification, the stratified liquid was moved to the separatory funnel, collecting the upper layer of biodiesel, and the excess methanol was recovered by depressurization concentration, and then cooled and weighed the biodiesel. Yields were calculated using the following equation¹¹

$$\text{yield (\%)} = m_{\text{biodiesel}}/m_{\text{seed oil}} \times 100\%$$

4.2.5. TG-DTG Analysis of Seed Oil and Biodiesel. A Q50-type thermogravimetric analyzer (TA Instruments, New Castle DE, State of Delaware) was used to test the thermal mass loss of the sample. Under nitrogen protection, the temperature was increased at 10 °C/min between 50 and 600 °C to measure the mass loss of the sample and examine its thermal stability.

4.2.6. FT-IR Analysis of Seed Oil and Biodiesel. The samples were prepared by tableting with KBr and analyzed using an IS10-type Fourier transform infrared (FT-IR) spectrophotometer (Nicolet, MA) in the wavelength range 400–4000 cm^{-1} .

4.2.7. GC-MS Analysis of Biodiesel. The main components of the biodiesel, such as fatty acid methyl esters, were quantitatively determined by GC-MS (Agilent Technologies, Palo Alto, CA) with a capillary column (30 m \times 0.25 mm, film thickness 0.25 μm) and a mass selective detector (Agilent 6890N-5973) operated in the electron ionization mode. The sample (1 μL) was injected manually in the splitless mode. The injector temperature was 250 °C and the detector temperature was 260 °C. The carrier gas was helium at a flow rate of 1 mL/min. The oven temperature was increased from 20 to 80 °C at 5 °C/min, held at 80 °C for 1.0 min, and increased from 80 to

250 °C at a rate of 5 °C/min. The MS was operated at 70 eV with a scan range of 10–1000 amu. The chemical compositions of the biodiesels were determined by direct comparison of their mass spectra with those in the NIST11 Mass Spectral Library.

4.2.8. Calorific Value Analysis of Seed Oil and Biodiesel. The calorific value was tested by the Digital Display Oxygen Bomb Calorimeter (XRY-1A) purchased from Shanghai Hengqin Instrument Equipment Co., Ltd. (Shanghai, China). A known amount of fuel was placed in the crucible. The crucible was then placed over a ring, and a fine magnesium wire touching the fuel sample was stretched across the electrodes. The lid was tightly screwed on and the bomb was filled about 25 atm of pressure with O₂. The initial temperature was recorded. After completion of the circuit, the fuel in the crucible burned with the evolution of heat, and the maximum temperature attained was recorded.

■ ASSOCIATED CONTENT

SI Supporting Information

The Supporting Information is available free of charge at <https://pubs.acs.org/doi/10.1021/acsomega.1c00504>.

GC-MS spectra and composition data of seed oil and biodiesel are shown Figures S1, S2, and Tables S1, S2 (PDF)

■ AUTHOR INFORMATION

Corresponding Authors

Chunhui Ma – Key Laboratory of Bio-based Material Science and Technology (Ministry of Education), Northeast Forestry University, 150040 Harbin, China; orcid.org/0000-0001-9590-3891; Phone: +86-451-82191204; Email: mchmchmchmch@163.com

Shouxin Liu – College of Material Science and Engineering, Northeast Forestry University, 150040 Harbin, China; orcid.org/0000-0002-0491-8885; Phone: +86-451-82191204; Email: liushouxin@126.com; Fax: +86-451-82191502

Authors

Jintao Yu – Key Laboratory of Bio-based Material Science and Technology (Ministry of Education), Northeast Forestry University, 150040 Harbin, China

Yinhang Wang – College of Material Science and Engineering, Northeast Forestry University, 150040 Harbin, China

Luqi Sun – College of Material Science and Engineering, Northeast Forestry University, 150040 Harbin, China

Zhou Xu – College of Material Science and Engineering, Northeast Forestry University, 150040 Harbin, China

Yadong Du – College of Material Science and Engineering, Northeast Forestry University, 150040 Harbin, China

Huiliang Sun – College of Material Science and Engineering, Northeast Forestry University, 150040 Harbin, China

Wei Li – Key Laboratory of Bio-based Material Science and Technology (Ministry of Education), Northeast Forestry University, 150040 Harbin, China; orcid.org/0000-0002-3008-9865

Sha Luo – College of Material Science and Engineering, Northeast Forestry University, 150040 Harbin, China

Complete contact information is available at:

<https://pubs.acs.org/doi/10.1021/acsomega.1c00504>

Funding

All authors have declared that: (i) no support, financial or otherwise, has been received from any organization that may have an interest in the submitted work and (ii) there are no other relationships or activities that could appear to have influenced the submitted work.

Notes

The authors declare no competing financial interest.

■ ACKNOWLEDGMENTS

This research was supported by the National Natural Science Foundation of China (grant number 31890773) and the Fundamental Research Funds for the Central Universities (2572019BB02). We thank Gabrielle David, Ph.D., from Liwen Bianji, Edanz Group China (www.liwenbianji.cn/ac), for editing the English text of a draft of this manuscript.

■ REFERENCES

- (1) Lewis, N. S. Research opportunities to advance solar energy utilization. *Science* **2016**, *351*, No. aad1920.
- (2) Nocera, D. G. Chemistry of personalized solar energy. *Inorg. Chem.* **2009**, *48*, 10001–10017.
- (3) Lee, Y. H.; Kim, J. S.; Noh, J.; Lee, I.; Kim, H. J.; Choi, S.; Seo, J.; Jeon, S.; Kim, T. S.; Lee, J. Y.; Choi, J. W. Wearable textile battery rechargeable by solar energy. *Nano Lett.* **2013**, *13*, 5753–5761.
- (4) Ollitrault, J.-Y.; Gardim, F. G. Hydro overview. *Nucl. Phys. A* **2013**, *904–905*, 75c–82c.
- (5) Rourke, F. O.; Boyle, F.; Reynolds, A. Tidal energy update 2009. *Appl. Energy* **2010**, *87*, 398–409.
- (6) Kaldellis, J. K.; Zafirakis, D.; Stavropoulou, V.; Kaldelli, E. Optimum wind- and photovoltaic-based stand-alone systems on the basis of life cycle energy analysis. *Energy Policy* **2012**, *50*, 345–357.
- (7) Bechtle, P.; Schelbergen, M.; Schmehl, R.; Zillmann, U.; Watson, S. Airborne wind energy resource analysis. *Renewable Energy* **2019**, *141*, 1103–1106.
- (8) Kale, D. Geothermal energy. *Proc. Indian Natl. Sci. Acad.* **2015**, *81*, 993–999.
- (9) Swain, P. K.; Das, L. M.; Naik, S. N. Biomass to liquid: A prospective challenge to research and development in 21st century. *Renewable Sustainable Energy Rev.* **2011**, *15*, 4917–4933.
- (10) Wobiwo, F. A.; Emaga, T. H.; Fokou, E.; Boda, M.; Gillet, S.; Deleu, M.; Richel, A.; Gerin, P. A. Comparative biochemical methane potential of some varieties of residual banana biomass and renewable energy potential. *Biomass Convers. Biorefin.* **2017**, *7*, 167–177.
- (11) Shah, S. N.; Pranesh, M.; Raj, J. J.; Mutalib, M. I. A.; Lethesh, K. C.; Ghanem, O. B.; Ullahbe, Z. De-acidification of crude oil using supported ionic liquids phases. *Sep. Purif. Technol.* **2018**, *196*, 96–105.
- (12) Hancsók, J.; Sági, D.; Valyon, J. Diesel fuel blending components from mixture of waste animal fat and light cycle oil from fluid catalytic cracking. *J. Environ. Manage.* **2018**, *223*, 92–100.
- (13) Chen, R.-X.; Wang, W. C. The production of renewable aviation fuel from waste cooking oil. Part I: Bio-alkane conversion through hydro-processing of oil. *Renewable Energy* **2019**, *135*, 819–835.
- (14) Shah, Z.; Veses, R. C.; Vaggetti, J. C. P.; Amorim, V. D. A.; Silva, R. D. Preparation of jet engine range fuel from biomass pyrolysis oil through hydrogenation and its comparison with aviation kerosene. *Int. J. Green Energy* **2019**, *16*, 350–360.
- (15) Lilik, G. K.; Boehman, A. L. Advanced diesel combustion of a high cetane number fuel with low hydrocarbon and carbon monoxide emissions. *Energy Fuels* **2011**, *25*, 1444–1456.
- (16) Han, W.-Q.; Yao, C.-D. Research on high cetane and high octane number fuels and the mechanism for their common oxidation and auto-ignition. *Fuel* **2015**, *150*, 29–40.
- (17) Baldwin, L. C.; Davis, M. C.; Hughes, A. M.; Lupton, D. V. Potential Vegetable-Based Diesel Fuels from Perkin Condensation of

Furfuraldehyde and Fatty Acid Anhydrides. *J. Am. Oil Chem. Soc.* **2019**, *96*, 571–583.

(18) Atadashi, I. M.; Aroua, M. K.; Abdul Aziz, A. R.; Sulaiman, N. M. N. The effects of water on biodiesel production and refining technologies: A review. *Renewable Sustainable Energy Rev.* **2012**, *16*, 3456–3470.

(19) Borges, M. E.; Díaz, L. Recent developments on heterogeneous catalysts for biodiesel production by oil esterification and transesterification reactions: A review. *Renewable Sustainable Energy Rev.* **2012**, *16*, 2839–2849.

(20) Atabani, A. E.; Cesar, A. S. *Calophyllum inophyllum* L.- A prospective non- edible biodiesel feedstock. Study of biodiesel production, properties, fatty acid composition, blending and engine performance. *Renewable Sustainable Energy Rev.* **2014**, *37*, 644–655.

(21) Baldwin, L. C.; Davis, M. C.; Woodroffe, J. D. Potential oxygenated biofuels synthesized from fusel pentanols. *Fuel* **2020**, *270*, 117505–117512.

(22) Ullah, Z.; Bustam, M. A.; Man, Z.; Khan, A. S.; Muhammad, N.; Sarwono, A.; Farooq, M.; Ullah, R.; Mengal, A. N. A detail description on catalytic conversion of waste palm cooking oil into biodiesel and its derivatives: new functionalized ionic liquid process. *ChemistrySelect* **2017**, *2*, 8583–8595.

(23) Karimi, B.; Vafaezadeh, M. SBA-15-functionalized sulfonic acid confined acidic ionic liquid: a powerful and water-tolerant catalyst for solvent-free esterifications. *Chem. Commun.* **2012**, *48*, 3327–3329.

(24) Su, F.; Guo, Y. Advancements in solid acid catalysts for biodiesel production. *Green Chem.* **2014**, *16*, 2934–2957.

(25) Kouzu, M.; Hidaka, J. Transesterification of vegetable oil into biodiesel catalyzed by CaO: A review. *Fuel* **2012**, *93*, 1–12.

(26) Man, Z.; Elsheikh, Y. A.; Bustam, M. A.; Yusup, S.; Mutalib, M. I. A.; Muhammad, N. A Brønsted ammonium ionic liquid-KOH two-stage catalyst for biodiesel synthesis from crude palm oil. *Ind. Crops and Prod.* **2013**, *41*, 144–149.

(27) Macario, A.; Giordano, G. Catalytic Conversion of Renewable Sources for Biodiesel Production: A Comparison Between Biocatalysts and Inorganic Catalysts. *Catal. Lett.* **2013**, *143*, 159–168.

(28) Zhang, D.; Duan, M.; Yao, X.; Fu, Y.; Zu, Y. Preparation of a novel cellulose-based immobilized heteropoly acid system and its application on the biodiesel production. *Fuel* **2016**, *172*, 293–300.

(29) Liu, H.; Su, L.; Liu, F.; Li, C.; Solomon, U. U. Cinder supported K₂CO₃ as catalyst for biodiesel production. *Appl. Catal., B* **2011**, *106*, 550–558.

(30) Zabeti, M.; Wan, M.; Aroua, M. K. Activity of solid catalysts for biodiesel production: A review. *Fuel Process. Technol.* **2009**, *90*, 770–777.

(31) Oshima, T.; Sakamoto, T.; Ohe, K.; Baba, Y. Cellulose aerogel regenerated from ionic liquid solution for immobilized metal affinity adsorption. *Carbohydr. Polym.* **2014**, *103*, 62–69.

(32) Li, X.; Zhao, D.; Fei, Z.; Wang, L. Applications of functionalized ionic liquids. *SciChina. Ser. B.* **2006**, *49*, 385–401.

(33) Amarasekara, A. S. Acidic Ionic Liquids. *Chem. Rev.* **2016**, *116*, 6133–6183.

(34) Goossens, K.; Lava, K.; Bielawski, C. W.; Binnemans, K. Ionic Liquid Crystals: Versatile Materials. *Chem. Rev.* **2016**, *116*, 4643–4807.

(35) Ma, C.; Liu, T.; Yang, L.; Zu, Y.; Wang, S.; Zhang, R. Study on ionic liquid-based ultrasonic-assisted extraction of biphenyl cyclo-octene lignans from the fruit of *Schisandra chinensis* Baill. *Anal. Chim. Acta* **2011**, *689*, 110–116.

(36) Zhu, Z.; Hu, J.; Geng, X.; Qin, B.; Ma, K.; Wang, Y.; Gao, J. Process design of carbon dioxide and ethane separation using ionic liquid by extractive distillation. *J. Chem. Technol. Biotechnol.* **2018**, *93*, 887–896.

(37) Stockmann, T. J.; Boyle, P. D.; Ding, Z. Preparation and crystal structure of tetraoctylphosphonium tetrakis (pentafluorophenyl) borate ionic liquid for electrochemistry at its interface with water. *Catal. Today* **2017**, *295*, 89–94.

(38) Vafaezadeh, M.; Hashemi, M. M. Efficient fatty acid esterification using silica supported Brønsted acidic ionic liquid catalyst: Experimental study and DFT modeling. *Chem. Eng. J.* **2014**, *250*, 35–41.

(39) Muhammad, N.; Elsheikh, Y. A.; Mutalib, M. I. A.; Bazmi, A. A.; Khan, R. A.; Khan, H.; Rafiq, S.; Man, Z.; Khan, I. An overview of the role of ionic liquids in biodiesel reactions. *J. Ind. Eng. Chem.* **2015**, *21*, 1–10.

(40) Vafaezadeh, M.; Karbalaie-Reza, M.; Hashemi, M. M.; Soleimany, K. Q. Surfactant-like Brønsted acidic ionic liquid as an efficient catalyst for selective Mannich reaction and biodiesel production in water. *J. Iran. Chem. Soc.* **2017**, *14*, 907–914.

(41) Sun, S.; Li, X. Functional Ionic Liquids Catalyzed the Esterification of Ricinoleic Acid with Methanol to Prepare Biodiesel: Optimization by Response Surface Methodology. *J. Am. Oil Chem. Soc.* **2016**, *93*, 757–764.

(42) Zheng, X.; He, L.; Duan, Y.; Jiang, X.; Xiang, G.; Zhao, W.; Zhang, S. Poly (ionic liquid) immobilized magnetic nanoparticles as new adsorbent for extraction and enrichment of organophosphorus pesticides from tea drinks. *J. Chromatogr. A* **2014**, *1358*, 39–45.

(43) Pereira, M. M. A. Immobilized ionic liquids in organic chemistry. *Curr. Org. Chem.* **2012**, *16*, 1680–1710.

(44) He, Y.; Zhang, Q.; Zhan, X.; Cheng, D. G.; Chen, F. Novel Immobilized Ionic Liquid Catalysts based on Micro/Mesoporous Materials. *Chem. Lett.* **2016**, *46*, 215–217.

(45) Fang, L.; Tian, M.; Yan, X.; Xiao, W.; Row, K. H. Dual ionic liquid-immobilized silicas for multi-phase extraction of aristolochic acid from plants and herbal medicines. *J. Chromatogr. A* **2019**, *1592*, 31–37.

(46) Zheng, X.; Luo, S.; Zhang, L.; Cheng, J. P. Magnetic nanoparticle supported ionic liquid catalysts for CO₂ cycloaddition reactions. *Green Chem.* **2009**, *11*, 455–485.

(47) Zhang, Y.; Xia, C. Magnetic hydroxyapatite-encapsulated gamma-Fe₂O₃ Nanoparticles functionalized with basic ionic liquids for aqueous Knoevenagel condensation. *Appl. Catal., A* **2009**, *366*, 141–147.

(48) Taher, A.; Jin-Beom, K. K.; Jung, J. Y.; Ahn, W. S.; Jin, M. J. Highly active and magnetically recoverable Pd-NHC catalyst immobilized on Fe₃O₄ nanoparticle-ionic liquid matrix for Suzuki reaction in water. *Synlett.* **2009**, *15*, 2477–2482.

(49) Jiang, Y.; Guo, C.; Xia, H.; Mahmood, I.; Liu, C.; Liu, H. Magnetic nanoparticles supported ionic liquids for lipase immobilization: Enzyme activity in catalyzing esterification. *J. Mol. Catal. B: Enzym.* **2009**, *58*, 103–109.